This document is the Accepted Manuscript version of a Published Work that appeared in final form in **Sensors and Actuators B: Chemical**, copyright © Elsevier Inc. after peer review and technical editing by the publisher. To access the final edited and published work see [https://doi.org/10.1016/j.snb.2016.09.124].

Features of the use of optical reflection from thin porous silicon for the detection of organic liquids

Nickolai I. Klyui[1,3], Ivan I. Ivanov[2,4], Oleksandr S. Kyslovets[2], Lyubov V. Avksentyeva[3], and Valeriy A. Skryshevsky[2,5]

[1]*College of Physics, Jilin University, Changchun, 130012, PR China*
[2]*Institute of High Technologies, Taras Shevchenko National University of Kyiv, 64 Volodymyrska, 01033 Kyiv, Ukraine*
[3]*V. Lashkaryov Institute of Semiconductor Physics, National Academy of Sciences of Ukraine, 41 Prosp. Nauky, Kyiv 03680, Ukraine*
[4]*ivancko@gmail.com*
[5]*skrysh@univ.kiev.ua*

Abstract: The rapid technique to define the thickness and rate of porous silicon (PS) layers growth during the electrochemical etching of silicon wafer is suggested. The method is based on the in situ measurement of reflected laser beam from PS layer in cell with electrolyte during the etching process. Numerical simulation of interference data obtained from the reflectivity on wavelength dependence shows the possibility to improve the selectivity of thin layer PS sensor using the set of PS layers with defined thicknesses and porosities. The different behavior of the reflection coefficients, shape and position of the maxima for the interference peaks of the PS film during desorption of water-ethanol solutions and wines are observed at the using PS layer as an optical sensor. Such differences in the peak shape indicate the presence of inhomogeneity in the distribution of the film porosity with depth. On the other hand, the difference in the nature of interaction between the adsorbed molecules with the pore`s surface causes differences in the kinetics of the change of the optical characteristics during desorption. It should be taken into consideration at the development of optical sensors based on porous materials.

Key words Adsorption/desorption; Thin films; Porous silicon; Chemical sensors; Spectroscopy.

1. Introduction

Optical properties of porous silicon (PS) have been proposed for gas, vapor and liquid sensing since they were found to be extremely sensitive to the presence of dielectric substances inside of the pores [1, 2]. The effective refractive index of the PS layer increases at the pore filling, shifting the optical spectrum of the layer to longer wavelengths. Thus, by monitoring the reflectance or transmission spectrum, one can detect the binding of molecules inside the pores. In order to control the refractive index of the PS samples, a convenient way is to fabricate the samples as stacks of thin layers such as a Bragg mirror, rugate filter, Fabry–Perot filter, luminescent PS microcavity [3-8]. Bragg mirrors are periodic stacks of two quarter-wavelength optical thickness layers of different refractive indices. The periodicity gives rise to a photonic bandgap, in which light propagation is forbidden and incident light is reflected. A microcavity consists of two Bragg mirrors and a layer that breaks the periodicity of the

refractive index profile. The reflectance spectrum of the microcavity with a half-wavelength optical thickness layer is characterized by a resonant dip in the stop band. Due to such optical tuning multilayers structures reveal high sensing to different liquids and gases. The sensitivity of optical sensors is $\Delta\lambda/\Delta n$, where $\Delta\lambda$ is the wavelength shift and Δn is the change of refractive index. For a system able to detect a wavelength shift of 0.1 nm, the minimum detectable refractive index change is 2.10^{-4} [9]. The problem of PS optic sensors is the instability due to the aging of PS itself. One way to prevent this effect is the PS oxidation [10] or PS chemical modification [11].

In general, single layers with thickness when the interference pattern is observed also can be an effective sensors. Nevertheless, it is considered that their sensitivity is less comparing with multilayers structures due to wide peak comparing with multilayer structures. However, at the studying of kinetics characteristics like adsorption/desorption process the single layer application is preferable due to more simple result interpretation. Unfortunately, both single and multilayers PS structures display bed selectivity to molecule of interest. Usually, the selectivity such sensors achieves via supplementary surface functionalization. The porous surface is covered by functional groups that react separately with a specific type of molecules. Such approach is widely use for biosensors, like enzim-substrate, antibody-antigen, DNA, etc [12-14]. However, for nonorganic and organic liquids recognition such way is not applicable.

At creation of the PS by electrochemical etching of Si wafer the important role should play the parameter`s control of the grown layer. Of course, the parameters of the PS can be evaluated at the end of the process by the measuring of reflection spectrum or by elipsometry [15]. However, it is desirable to have the ability to control the parameters of the individual layers of the PS during growth in situ and, if necessary, to govern the growth process.

In present work is proposed the express method to determine the parameters of thin growing layer of PS on Si substrate. The method is based on the *in situ* measurement of reflection spectra of growing layer at electrochemical etching of Si. The steady state and kinetic spectral dependences of reflectance of PS sensor structures was analyzed by numerical simulation and experimentally. Method of improvement of optical sensors base on PS interference pattern is proposed.

2. Materials and methods

The design of the measuring system shown in Fig. 1. The modulated laser beam falls on the silicon substrate, which is placed into specially designed teflon cell. The shoulder with laser can be rotated in a vertical plane, that allows us to change the angle of incidence for the laser beam on the substrate. In the teflon cell with $HF:H_2O:C_2H_5OH$ electrolyte the electrochemical etching of silicon occurs at applying of anodic potential to Si substrate. The laser beam of λ=632 nm is reflected from multiple interfaces of the air – solution HF – dynamically formed layer of PS- silicon substrate. It should be noted that PS can be inhomogeneous with gradient refractive index.

The intensity if reflected beam is registered by photomultiplier, amplified and fed to the input of analog-to-digital converter (ADC) card and processed by developed software. Thus, with this setup it can monitor the intensity change of the reflected light from the structure during its growth (anodic etching).

The laser beam incidents on the sample under an angle θ_a. At time t_0, when the electrochemical etching of silicon plates (with thickness d) begins, the thickness of the PS layer is equal to zero. For $t>t_0$ on the frontier of the HF solution - silicon the PS layer is formed, its thickness increases with time, simultaneously, the thickness of single crystal silicon is reduced. In general, the PS layer grows heterogeneously and each layer of PS has a refractive index n_i and thickness l_i. At the same time, the total thickness of the sample remains constant $d_{PS}+d_{Si}=d_{sample}=const$.

For experimental verification the silicon wafer with a resistivity ρ=0.001 Ω*cm was immersed in a 40% solution of alcohol and HF acid. Before etching the both background signal of photomultiplier and intensity of the reflected light from the sample under an angle of

45^0 in the absence of current (when the etching process does not occur) are registered. Experimental changes in the intensity of the laser beam reflected from the sample during the formation of PS layer was obtained for samples that were grown for 50 seconds at different current densities. The change in anode current corresponds to the etching with different speed of porous layer growth [16]. Fig. 2a shows the reflection versus time for structure with j=36 mA/cm^2.

Dependence R=f(t) (at λ=const) reveals interference maxima if the phase difference of the beams reflected from front and rear boundaries of the PS layer is equal to nπ (n=0, 1, 2,…). Then the thickness d_{PS} at which the maximum arises can be written as:

$$d_{PS} = \frac{(2k+1)\lambda}{4n_{PS}\cos(\theta_a)},\ k=1,\ 2,.... \quad (1)$$

From this curve we can obtain the rate v_{PS} of porous silicon formation:

$$v_{PS} = \frac{d_{k+1} - d_k}{t_{k+1} - t_k} = \frac{\lambda}{2\Delta t n_{PS}\cos(\theta_a)} \quad (2)$$

Here t_{k+1}-t_k is time difference between neighbor maximum. At current density j=36 мА/см^2 and j=24 мА/см^2 the velocity of PS growth is 15.7 nm/s and 11 nm/s, which are in nice correlation with literature data [16]: with the decrease of the current growth the rate of porous silicon is reduced.

Since PS layer has a developed system of pores filled with air, so, pores can be filled with gases or liquids. In this work micro pipette dispenser ThermoFisher was used to deposit liquids analytes on samples.

A scanning electron microscope (SEM) and optical microsope was used to determine PS layers thiknesses and dependence of PS growth velosity on etching current density and etching time. Image of etched PS layer on Si wafer is shown in Fig. 2b. Si and PS layers are depicted by different shade of grey colour.

3. Numerical analysis

In order to calculate the reflection coefficient of formed structure let us consider the following model (Fig. 3).

The Snell's equations for border of two layers are the following:

$$n_a sin\theta_a = n_i sin\theta_i = n_b sin\ \theta_b,\ i=1,2,...M \quad (3)$$

where n_a is refractive index of air, n_i is refractive index of i-layer, n_b is refractive index of silicon wafer.

For each layer the δ_i phase thickness can be written as:

$$\delta_i = \frac{2\pi}{\lambda} n_i l_i \cos\theta_i = \frac{2\pi}{\lambda} n_i l_i \sqrt{1 - \frac{n_i^2 \sin^2\theta_a}{n_i^2}},\ i=1,2,...M \quad (4)$$

where λ is wavelength of light beam falling under angle θ_a on surface of layer, l_i is the thickness of i-layer.

The element coefficients of reflectivity ρ_{Ti} and transmission τ_{Ti} can be written as:

$$\rho_{Ti} = \frac{n_{T,i-1} - n_{T,i}}{n_{T,i-1} + n_{T,i}},\ i=1,\ 2,...,\ M+1 \quad (5)$$

$$\tau_{Ti} = 1 + \rho_{Ti},\ i=1,\ 2,...,\ M+1 \quad (6)$$

The border conditions are the followings:

$$n_{T0} = n_{Ta} \tag{7a}$$

$$n_{T,M+1} = n_{Tb} \tag{7b}$$

where n_{Ta} is air (left) side condition, n_{Tb} is wafer (right) condition.

$$n_{Ti} = \begin{cases} \dfrac{n_i}{\cos\theta_i}, \text{TM} - \textit{poliarisation} \\ n_i \cos\theta_i, \text{TE} - \textit{poliarisation} \end{cases}, \; i=a,\ 1,\ 2,\ldots,\ M,\ b \tag{8}$$

where θ_i is angle of light beam falling on i-border.

According to the matrix method the intermediate matrix can be written in order to calculate the coefficient of reflectivity of such multilayer structure. The last describes the components of electric field strength at the border between i and i+1 layers:

$$\begin{bmatrix} E_{Ti+} \\ E_{Ti-} \end{bmatrix} = \frac{1}{\tau_{Ti}} \begin{bmatrix} 1 & \rho_{Ti} \\ \rho_{Ti} & 1 \end{bmatrix} \begin{bmatrix} e^{j\delta i} & 0 \\ 0 & e^{-j\delta i} \end{bmatrix} \begin{bmatrix} E_{T,i+1,+} \\ E_{T,i+1,-} \end{bmatrix} \tag{9}$$

$$\begin{bmatrix} E_{T,M+1,+} \\ E_{T,M+1,-} \end{bmatrix} = \frac{1}{\tau_{T,M+1}} \begin{bmatrix} 1 & \rho_{T,M+1} \\ \rho_{T,M+1} & 1 \end{bmatrix} \begin{bmatrix} E'_{T,M+1,+} \\ 0 \end{bmatrix} \tag{10}$$

The coefficient of reflectivity Γ_i can be written using the next recursion formulas:

$$\Gamma_i = \frac{E_{Ti-}}{E_{Ti+}} = \frac{\rho_{Ti} + \Gamma_{T,i+1} e^{-2j\delta i}}{1 + \rho_{Ti}\Gamma_{T,i+1} e^{-2j\delta i}}, \; i=M,\ M\text{-}1,\ldots,\ 1 \tag{11}$$

The recursion is initialized via following equality:

$$\Gamma_{T,M+1} = \rho_{T,M+1} \tag{12}$$

Numerical simulation are fulfilled using the Eqs (3-12). The Bruggeman approximation was used for all simulation to specify the dependence between porosity and refraction index for PS as effective medium. The thickness of structure is changed in range of 0 - 2000 nm. The following parameters are chosen: n_{air}=1, HF solution (d=0.5 cm, n=1.33), PS (d=0-2000 nm, n=2), Si wafer (d=350-348 μm, n=3.5). The simulated dependence of reflection coefficient versus PS thickness is presented in Fig. 4.

The experimental curve (Fig.2) shows similar behavior to the dependence of reflection coefficient on thickness as calculated one (Fig.4). Not smooth experemental curve (Fig. 2) comparatively to computated one (Fig. 4) is conditioned by the evolution of hydrogen during the electrochemical etching of silicon [2].

3. Results and discussion

Deposition of liquid analyte on PS layer and subsequent pores filling leads to shift of interference maxima and minima peaks of air filled PS layer to long wave part of spectrum. For PS layer with specific porosity P=f($n_{Si}(\lambda)$) and thickness L_{PS} the position of some new maximum peak $\lambda^{i\max}_{PS(eth)}$ after pores filling by analyte (Fig. 5, curve b) can coincide with position of some minimum peak $\lambda^{i\min}_{PS(air)}$ of PS layer without analyte (Fig. 5, curve a). Reflectance increasing from $R^{i\min}_{PS(air)}$ to $R^{i\max}_{PS(eth)}$ is at wavelength $\lambda^{i\max}_{PS(eth)} = \lambda^{i\min}_{PS(air)}$ after pore filling with ethanol. Similarly for certain parameters of PS layer and analyte, reflectance

decreases from $R^{i\max}_{PS(air)}$ to $R^{i\min}_{PS(eth)}$ at points where minimum peak position of analyte filled PS layer coincides with maximum peak position of nonfilled PS layer ($\lambda^{i\max}_{PS(air)} = \lambda^{i\min}_{PS(eth)}$). Result on Fig. 5 is simulated for structure with PS layer thickness L_{PS}=500 nm, porosity P=70% and ethyl acohole as analyte.

Spectral dependence of reflectance of air, ethanol, methanol, ethylene glycol, methyl salicylate filled PS layer (thickness L_{PS}=500nm) for different porosity were simulated using matrix method, described above. Wavelength depended analytes refractive indexes were used for simulation [17]. Position of interference peaks of reflectance minima of air filled PS layer and position of and interference peaks reflectance maxima of analytes filled PS layers depicted in Fig. 6. Symbols □,○,◊,Δ in Fig. 6 show intersection point of peak minima curves for air filled pores with peak maxima curves for pores filled with different analytes: methanol, ethanol, ethylene glycol, methyl salicylate, respectively.

Each analyte has set of wavelength and porosity values for i- interference peak maxima $[\lambda\ P]^{i\max}_{analyte}$ and minima $[\lambda\ P]^{i\min}_{analyte}$ peaks, where $\lambda^{i\max}_{PS(analyte)} = \lambda^{i\min}_{PS(air)}$ and $\lambda^{i\max}_{PS(air)} = \lambda^{i\min}_{PS(analyte)}$, properly. Reflectance can be measured at points of these sets to detect selected analyte. Reflectance increasing of ethanol and methyl salicylate filled PS layer relatively to reflectance of nonfilled PS layer lies in range from 3 to 4000 (Fig. 7) at points mapped in Fig. 6.

Fixing the reflectance increasing directly to the determined values at all point of $[\lambda\ P]^{i\max}_{analyte}$ set and the reflectance decreasing directly to determined values at all point of $[\lambda\ P]^{i\min}_{analyte}$ set, we are able identify the specific analyte which located in the pores. Hereby, such set of PS structures with porosity $P^{i\max}_{analyte}$ and $P^{i\min}_{analyte}$ at wavelength $\lambda^{i\max}_{analyte}$ and $\lambda^{i\min}_{analyte}$ properly work as “optical switch” on this specific analyte.

Increasing of PS layer thickness L_{PS} from 300 nm to 1000 nm leads to increasing quantity of points where $\lambda^{i\max}_{PS(eth)} = \lambda^{i\min}_{PS(air)}$, and shifts these points to lower porosity. Fig. 8 depicts these dependences for PS layers filled with ethanol.

Thus, if you have a large set of samples of thin PS layers on silicon, there is a high probability that one of them will satisfy the above ratio and thus it is possible to assume what kind of the molecules are adsorbed. Beside such analysis allows us to improve the sensitivity of sensors. For fixed thickness of PS layer, there are discreet regions [P_{min}..P_{max}, λ_{min}…λ_{max}] where condition is satisfied for given set of analytes (Fig. 6). For example, set of samples with porosity P from P_{min}=58% to P_{max}=75% can be used to detect analytes as ethanol, methanol, ethylene glycole, methyl salicylate and other analytes with refractive indexes curves $n_{analyte}(\lambda)$ that lies between $n_{metanol}(\lambda)$ and $n_{Methyl\ Salicylate}(\lambda)$. Inside noticed region there is point with wavelength λ and porosity value P for which condition is satisfied for certain analyte. Porosity of silicon can be easy controlled with current density, and samples with discrete porosity about ΔP=1% or less can be grown. Number of discrete elements will be defined with possibilities of manufacturing process of PS with P_{min}, P_{max} and ΔP. One sample with porosity gradient grad(P)=ΔP/Δx can be used as alternative to set of samples with discrete porosity value. Sample with porosity gradient can be produced by using lateral constant voltage bias or using gradient profile of silicon wafer doping. Number of samples with discrete porosity can be limited and equal to number of detectable analyte if samples have optimal porosity to satisfy $\lambda^{i\max}_{PS(analyte)} = \lambda^{i\min}_{PS(air)}$ condition.

Computed sensitivity is $\Delta R/\Delta n=(R^{\max}_{PS(analyte)} - R^{\min}_{PS(air)})/(n_{analyte}-n_{air})=55..110$ at $\lambda^{i\max}_{PS(analyte)} = \lambda^{i\min}_{PS(air)}$ and depends on porosity, sensor structure thickness and wavelength.

As subject for study of kinetics of PS reflectance we selected ethanol, water, real alcohol drink as vodka (Nemiroff®, alcohol 40%), red wine (Cabernet, alcohol - 9.5%, sugar - 18 g/dm^3) and white wine (Cabernet, alcohol - 9..13%, sugar - 2..3 g/dm^3).

Analysis of tested liquids shows that liquids can be separated on two group: ethanol-containing liquids (ethanol, ethanol solutions, water as reference liquid) and sugar- containing liquids (red wine, white dry wine). First group of liquids has only one variable parameter – ethyl alcohol concertation. Second group has two variable parameters – ethyl alcohol concertation and sugar concentration. Water, vodka and ethanol form group of liquid with increasing concentration of ethanol. White wine and red wine form set with encreasing concentration of sugar. Liquids can be analyzed and compered only inside of their group.

Before the kinetics of adsorption–desorption processes of alcohol molecules in PS Bragg mirrors and microcavities were studied in [18-20]. In the present work the reflectance kinetics was measured from the single PS layer formed by electrochemical etching of p^+ Si (0.001 Ohm/cm) in 40%HF:C_2H_5OH:H_2O electrolyte for 9 sec at current 99 mA/cm^2. The PS thickness is about 700 nm, n_{eff} =2.65. Sample was washed with ethyl alcohol after each measurement and dryed using nitrogen flow. Control measurements of spectra after washing and drying showed the recovery of initial spectra.

Fig. 9 presents the experimental dependence of the reflection coefficient of the structure with nonfilled and filled by ethanol or water pores on the wavelength at different times after liquid deposition. By contarary to simulated spectra, the experimental refelectance peaks shows some shoulders due inhomogeneous growth of PS film. As can be seen, besides long wavelength shifting the observed spectra change the shape of an ideal sinusoid. It is noticeable especially at the adsorption of water, when some supplementary shoulders arise on main maxima. Such differences in the form indicate the presence of inhomogeneity in the distribution of the porosity of the film with depth. The origin of such transformation can be clarified from analysis of adsorption/desorption kinetics (Figs. 10, 11).

Adsorption/desorption kinetics of analyte as ethyl alcohol (Fig. 10), water (Fig. 11), vodka (Fig. 12), red wine (Fig. 13) and white wine (Fig. 14) were investigated. All measurement were performed with Thorlab CCD spectrometer CCS200. Speed of spectra measurements was 100 spectrum/s.

The initial position of the interference maximum of the peak is 560 nm. In the moment t_0 liquid analyte is deposited. Area B (t_0...t_1) corresponds to the transitional process associated with the spreading of analyte on the sample surface and filling the pores with molecules of analyte. After deposition of analyte is a dramatic shift of peak position λ_{peak} from λ^0_{peak} to $\lambda^{shift}_{peak} > \lambda^0_{peak}$. Value of shift is depended on analyte composition. At time t>t_1 is observed the desorption of molecules of analyte from the surface of the sample and from the pores which is accompanied by the returning of λ_{peak} to $\lambda_{peak} = \lambda^{0*}_{peak}$. Desorption of analyte molecules from sample surface doesn't lead to λ^{shift}_{peak} changing, desorption of analyte molecules from the pores leads to decreasing of λ^{shift}_{peak} as was described in our previous work [19]. If all molecules of analyte are desorbed from pores the condition is fullfilled: $\lambda^{0*}_{peak} = \lambda^0_{peak}$.

Creation of additional interference peak maxima is observed on Fig. 10 (zone D) and Fig 11-13 (zone C) due to the formation inside the pores of 2 regions – region with length of $W_{analyte}(t)$ which is still filled by analyte and the region with length of $W_{air}(t)$ which is already empty from molecules of analyte, as was described in our previous work [19]. In fact, there are 2 layers of PS with different effective refractive indices: $n_1=f(n_{Si}, n_{analyte})$ with length of

$W_{analyte}(t)$ and $n_2=f(n_{Si}, n_{analyte\ vapor}, n_{air})$ with length of $W_{air}(t)$. In the initial moment of time t_0 the $W_{analyte}(t)=0$, $W_{air}(t)=W_{PS}$. At time t_1 after complete pore filling: $W_{analyte}(t)=W_{PS}$, $W_{air}(t)=0$. In area werere desorption of analyte molecules from pores is observed: $W_{analyte}(t)$ tends to 0, and $W_{air}(t)$ tends to the W_{PS} with the condition $W_{analyte}(t)+W_{air}(t)=W_{PS}$=const (length of the pores).

Zone C (Fig. 10) corresponds to the desorption of ethanol molecules from the surface of the sample. In the area D ($t_2...t_3$) it is observed the desorption of molecules of ethyl alcohol from the pores which is accompanied by the returning of λ_{peak} to $\lambda_{peak}=\lambda^0_{peak}$. Since $\lambda_{peak(t_0)}=\lambda_{peak(t_3)}$ we can conclude that all the molecules of ethyl alcohol were desorbed from the pores. For water (Fig. 11), vodka (Fig. 12) , red wine (Fig. 13) and white wine (Fig. 14) zone C corresponds to the desorption of analyte molecules from the pores.

The arising and not disappearance of additional interference peak $\lambda^1_{peak}(t_2)=583$ nm (Fig. 11) shows that not all water molecules were desorbed from the pores.Vodka simplistically be regarded as a mixture of water and ethyl alcohol. For desorption of vodka, peak position is $\lambda_{peak}(t_2)$ =565 nm > $\lambda_{peak}(t_0)$=562 nm (Fig. 12). It is explained because not all molecules of vodka components were desorbed from the pores.

Analysis of dependences for ethyl alcohol (Fig. 10), water (Fig. 11) and vodka (Fig. 12) depict that λ^{shift}_{peak} (water)=602 nm < λ^{shift}_{peak} (vodka)=620 nm < λ^{shift}_{peak} (ethanol)=644 nm. Initial shift of the maximum position of the interference peak λ_{peak} after deposition of analytes on sample surface is depended on ethyl alcohol concentration in analyte. There are sub-regions on spectral dependences where two maximum peaks are exist simultaneously during desorption of analyte molecules from pores (region D on Fig. 10, region C on Fig. 11 and Fig. 12). Duration Δt of these sub-regions is proportion to the ethyl alcohol concentration in analyte: Δt_{ethyl}=3.2 s < Δt_{vodka}=15.4 s < Δt_{water}=57 s. Duration Δt_{water} was limited only by duration of measurement because not all water molecules are desorbed from the pores so two maximum peaks are observed and not disappear in time. For ethyl alcohol sensitivity $\Delta R/\Delta n$=67 was obtained. This experimental value lies in range of computed values.

Measured dependence of peak position λ^{shift}_{peak} on different concentrations of ethyl in ethyl-water mixture is shown on inset of Fig. 12. Peak shift is proportioned to ethyl portion in solution.Weak nonlinear dependence is observed due to nonlinear dependence of reflection coefficient of PS on porosity and nonlinear dependence of reflection coefficients of analytes on wavelenght. Received points form curve that can be used as calibration one to detect ethanol presence in solutions. Obtained value λ^{shift}_{peak} for vodka is in good accordance with values obtained for solutions of ethyl acohol and water.

In area C ($t_1...t_2$) it is observed the desorption of molecules of wine components from the pores (Fig.13, 14). Peak position $\lambda_{peak}(t_2)$ =570 nm>$\lambda_{peak}(t_0)$=561 nm for red wine (Fig. 13) and $\lambda_{peak}(t_2)$ =570 nm > $\lambda_{peak}(t_0)$=566 nm for white wine (Fig. 14). For red wine peak shift λ^{shift}_{peak} > λ^{shift}_{peak} for white wine, perhaps, because concentration of sugar in red wine (c_{sugar}=18 g/dm^3) is larger then in white wine (c_{sugar}=2..3 g/dm^3) and, respectively, the effective refractive index of red wine is larger comparatively to white wine.

Two maximum peaks were formed during desorption of red wine and remain all observation time. It is mainly due to the sugar molecules presence in pores after desorption of water an ethyl alcohol molecules. Wine consist from the following main components: water, ethanol, glycerol, organic acids, tannins, phenolics, nitrogenous compounds [21]. So, adsorption/desorption kinetic of wine is depended on wine components, interaction of wine components with pores walls and therefore is complicated process and require additional investigation.

Concentration of sugar in white dry wine is small - 2..3 g/dm^3 so white dry wine can be considered as only ethanol-containing liquid. Data point for white dry wine is little bit above the curve (Fig. 12, inset). It is explained presence of sugar and other organic components in this wine and therefore effective refraction coefficient of white dry wine is larger than effective refraction coefficient of ethanol-water solution with the same ethanol concentration.

It was analyzed also the kinetics of the changes of the reflection coefficient of PS samples with pored filled with analytes at wavelength that corresponds to the maximum of the interference peak $R(\lambda^0_{peak} = const)$. After deposition of analyte in moment t_0 onto the sample surface the value $R(\lambda^0_{peak}) = R(t_0)$ decreases to $R(t_1)$, where t_1 is time of ending of spreading of analyte on the sample surface. After beginning of desorption of molecules of analyte from pores $R(\lambda^0_{peak}) = R(t_1)$ increses to $R(t_3)$ for ethanol and to $R(t_2)$ for water, vodka, red and white whines. Time t_2 and t_3 is time at which the wavelength λ^{0*}_{peak} does not change for coresponded analytes. Ratio $R(t_0)/R(t_2)$, $R(t_0)/R(t_3)$ also characterizes the degree of desorption of molecules of analytes from the pores. Ratio $R(t_0)/R(t_2)$, $R(t_0)/R(t_3)$ equals 1 for complete desorption of molecules of analyte from pores.

Parametrs of analyse of adsorption/desorption kinetics of analytes are shown in Table 1.

Values of characteristic parameters of adsorbtion/desorption kinetics curves are collected in the Table 1. Characteristic parameters as λ^{shift}_{peak}, $R(t_0)/R(t_1)$, $R(t_0)/R(t_2)$ show direct dependence on variable parameters of analyte liquids inside liquid group.

Table 1

Analyte	Ethyl. alcohol, %	Sugar, g/dm^3	λ^0_{peak}, nm	λ^{shift}_{peak}, nm	Peak 0 λ^{0*}_{peak}, nm	Peak 1 λ^1_{peak}, nm	At $\lambda^0_{peak} = const$	
							$\frac{R(t_0)}{R(t_1)}$	$\frac{R(t_0)}{R(t_2)}$, $\frac{R(t_0)}{R(t_3)}$ (Note: t_3 - for ethyl, t_2 - for vodka, water, wines)
Ethyl alcohol	96	0	560	644	560		7.7	0.99
Vodka	40	0	560	620	565		6.7	0.92
Water	0	0	560	602	563	587	5.1	0.9
White wine	9..13	2..3	560	611	566		12	0.7
Red wine	9.5	18	560	631	570	591	9.7	0.67

Occurrence of additional interference peak maximum $\lambda^1_{peak} > \lambda^{0*}_{peak}$ after completion of the desorption of analyte molecules from pores depicts that analyte molecules form layer with sharp interface on the bottom of the pores [19]. There is sharp inteface betwean part of pore filled with residual of analyte molecules and part of pore filled with air. Presence of single interference peak maximum $\lambda^{0*}_{peak} > \lambda^0_{peak}$ after completion of the desorption of analyte molecules from pores depicts that residual of analyte molecules are homogeneously are adsorbed on all internal surface of pores. In practice these two profiles of pores filling with residual of analyte molecules can exist simultaniously and ratio $R(t_0)/R(t_2)$, $R(t_0)/R(t_3)$ can take values less then 1.

Archer et al. (2005) shows that real-time measurements of electrical parameters as C and G or optical parameters as reflectance coefficient are more informative compared to steady

measurements. Analysis of adsorption/desorption kinetics curves shows that both optical and electrical method of PS sample investigation has common stages in the response: exposure (addition of the analyte on PS layer surface), stabilization (transient process caused transient process caused infiltration analyte into pores), evaporation of analyte from PS layer surface, evaporation of analyte from PS pores. Investigation of the response of the PS sensor on deposited on PS layer volume of analyte shows that volume of analyte effects on time when surface is wet (time of analyte evaporation from surface) but doesn't effect on sensor response for both measurement methods. Chemical adsorption of analyte molecules on PS wals inside pores can cause not completely reversible process of analyte desorption from pores and not returning of measured values to its original value for both methods. Results received by electrical methods are depend on dipole moment, dielectric constant of the analyte molecules and alignment of analyte molecule dipoles [Archer and all, 2005]. Results received by optical methods are depend on dielectric constant of the analyte molecules. Optical method of sample investigation is more simple because metal contacts is not necessary and adsorption/desorption kinetics can be investigated simultaneously for wavelength in wide spectral range using CCD spectrometers.

Peculiarities of adsorbtion/desorption kinetics of analyte depend on mechanisms of interaction of the analyte molecules with the walls of the PS pores and the analyte molecules themselves. Thus, peculiarities of adsorbtion/desorption kinetics should be taken into consideration at the development of optical sensors on porous silicon since provide supplementary data about adsorption/desorption processes during the optical sensor operation.

4. Conclusion

This paper describes an automated system for in-situ control of the growth parameters of thin PS layers. The complex allows to determine the growth rate of PS layers as well as to track changes in the rate of growth of the PS over time. The experimental results showed that there is a good agreement with the results of computer simulation.

Dependences of reflectance of air, ethanol, methanol, ethylene glycol, methyl salicylate filled PS layers on porosity (P) and wavelength shows presence of sets [P, λ] where peak minima and maxima position of non filled PS layer equal to peak maxima and minima position of filled by analyte PS layer, respectively. Set of PS structures with computed discrete porosity and analysis of reflectance responses at simulated discrete wavelengths can be used to create multisensors array for electronic nose. It seems, it is attractive approach to create cheap electronic nose on the base of set of single PS layer structures. Peculiarities of water, ethanol, vodka, red and white wine adsorbtion/desorption kinetics at the in situ measurement of reflectance spectra of single PS layer should be taken into consideration for optical sensor operation.

Acknowledgments

This work was supported by the national long-term project No WQ20142200205 of "Thousand Talents Plan of Bureau of Foreign Experts Affairs" of the People's Republic of China, Programme H2020-MSCA-RISE-2015 (Project 690945 "Carther") and Ministry of Education and Science of Ukraine.

References

1. M. J. Sailor, Porous silicon in Practice. Preparation, Characterisation and Application (Wiley-VCH, 2012)
2. O. Bisi, S. Ossicini, and L. Pavesi, "Porous silicon: a quantum sponge structure for silicon based optoelectronics," Surf. Sci. Rep 38, 1-126 (2000).
3. I. A. Levitsky, "Porous Silicon Structures as Optical Gas Sensors," Sensors, 15, 19968–19991 (2015).

4. L. D. Stefano, K. Malecki, F. G. Della Corte, L. Moretti, I. Rea, and I. Rendina, “A Microsystem Based on Porous Silicon-Glass Anodic Bonding for Gas and Liquid Optical Sensing,” Sensors 6, 680-687 (2006).
5. H. Min, H. Yang, and S. Cho, “Extremely sensitive optical sensing of ethanol using porous silicon,” Sens. Actuators B 67. 199–202 (2000).
6. M. Ghulinyan, C. J. Oton, G. Bonetti, Z. Gaburro, and L. Pavesi, “Free-standing porous silicon single and multiple optical cavities,” J. Appl. Phys. 93, 9724-2729 (2003).
7. D. J. Gargas, O. Muresan, D. J. Sirbuly, and S. K. Buratto, “Micropatterned Porous-Silicon Bragg Mirrors by Dry-Removal Soft Lithography,” Adv. Mater. 18, 3164–3168 (2006).
8. G. Korotcenkov and B. Cho, “Porous semiconductors: advanced materials for gas sensor application,” Critic. Rev. Solid State Mater. Sci. 35, 1-37 (2010).
9. H. Ouyang and P. M. Fauchet, “Biosensing Using Porous Silicon Photonic Bandgap Structures,” in Photonic Crystals and Photonic Crystal Fibers for Sensing Applications, H. H. Du, ed. (SPIE, 2005), pp. 600508 1-15.
10. P. Bettotti, M. Cazzanelli, L. Dal Negro, B. Danese, Z. Gaburro, C. J. Oton, G. V. Prakash, and L. Pavesi, “ Silicon nanostructures for photonics,” J. Phys.: Condens. Matter. 14, 8253–8281 (2002).
11. M. Rocchia, E. Garrone, F. Geobaldo, L. Boarino, and M. J. Sailor, “Sensing CO_2 in a chemically modified porous silicon film,” Phys. Stat. Solidi A 197(2), 365–369 (2003).
12. V. S. Lin, K. Motesharei, K. S. Dancil, M. J. Sailor,and M. R. Ghadiri, “A Porous Silicon-Based Optical Interferometric Biosensor,” Science 278, 840-843 (1997).
13. M. P. Stewart and J. M. Buriak, “Chemical and Biological Applications of Porous Silicon Technology,” Adv. Mater. 12(12), 859-869 (2000).
14. S. Chan, Y. Li, L. J. Rothberg, B. L. Miller, and P. M. Fauchet, “Nanoscale silicon microcavities for biosensing,” Mater. Sci. Eng. C 15(1-2), 277–282 (2001).
15. G.Wang, and H. Arwin, “Modification of vapor sensitivity in ellipsometric gas sensing by copper deposition in porous silicon,” Sens. Actuators B-Chem. 85(1-2), 95-103 (2002).
16. L. Canham, Handbook of Porous silicon (Springer, 2014).
17. S. Kedenburg, M. Vieweg, T. Gissibl, and H. Giessen, “Linear refractive index and absorption measurements of nonlinear optical liquids in the visible and near-infrared spectral region,” http://refractiveindex.info.
18. Z. Gaburro, N. Daldosso, L. Pavesi, G. Faglia, C. Baratto, and G. Sberveglieri, “Monitoring penetration of ethanol in a porous silicon microcavity by photoluminescence interferometry,” Appl. Phys. Lett. 78, 3744-3746 (2001).
19. I. I. Ivanov, V. A. Skryshevsky, T. Serdiuk, and V. Lysenko, “Kinetics of adsorption–desorption processes of alcohol molecules in porous silicon Bragg mirror,” Sens. Actuators B-Chem. 174, 521-526 (2012).
20. L. Stefano, L. Moretti, I. Rendina, and A.M. Rossi, “Time-resolved sensing of chemical species in porous silicon optical microcavity,” Sens. Actuators B-Chem. 100(1-2), 168–172 (2004).
21. H.-F. Linskens, J. F. Jackson, Wine Analysis (Springer Berlin Heidelberg, 1988).

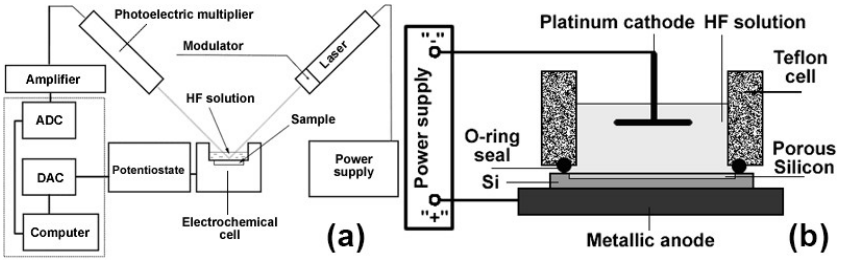

Fig.1 a) Schema of measurement of reflected light during PS growing on Si substrate; b) experimental setup of electrochemical cell for PS fabrication.

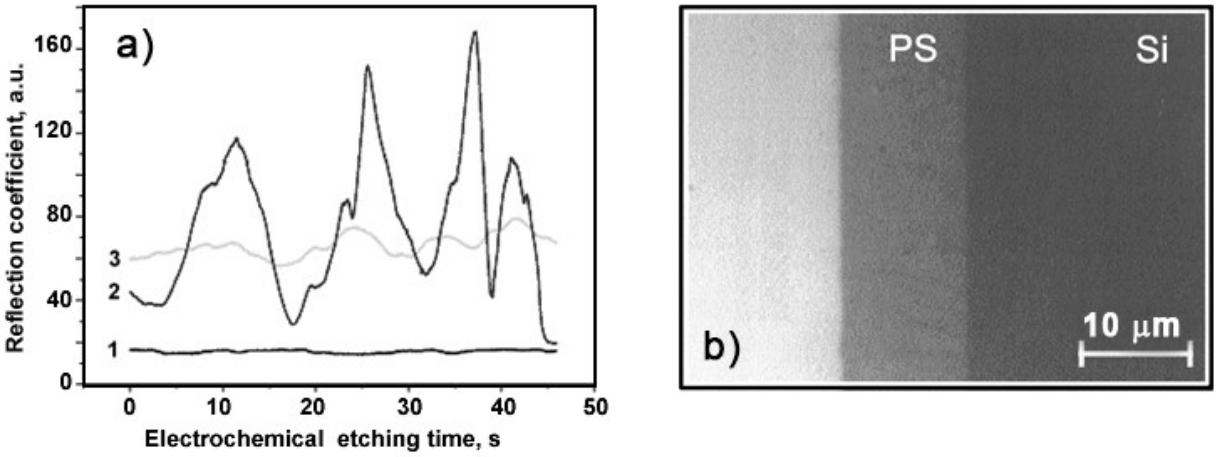

Fig. 2. a) Dependence of intensity of reflected laser beam from time: 1- background signal of photomultiplier; 2 – signal from sample during etching process: 3 –signal from sample (without etching); b) microscope image of PS layer on Si wafer.

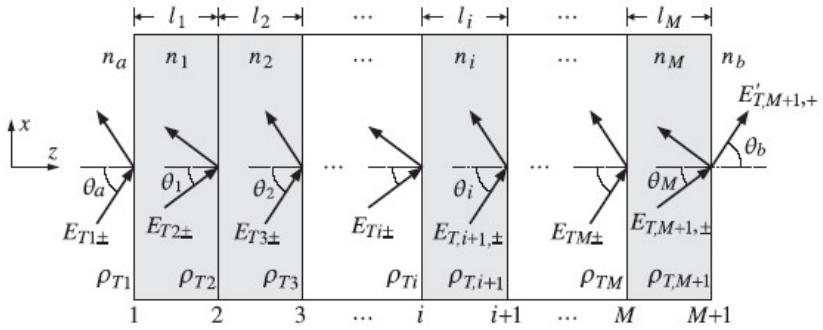

Fig. 3. Multilayer structure on which laser beam falls under angle θ_a .

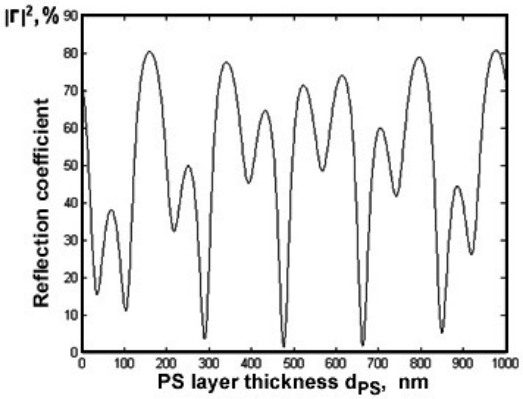

Fig. 4. Simulated dependence of reflection coefficient on PS thickness.

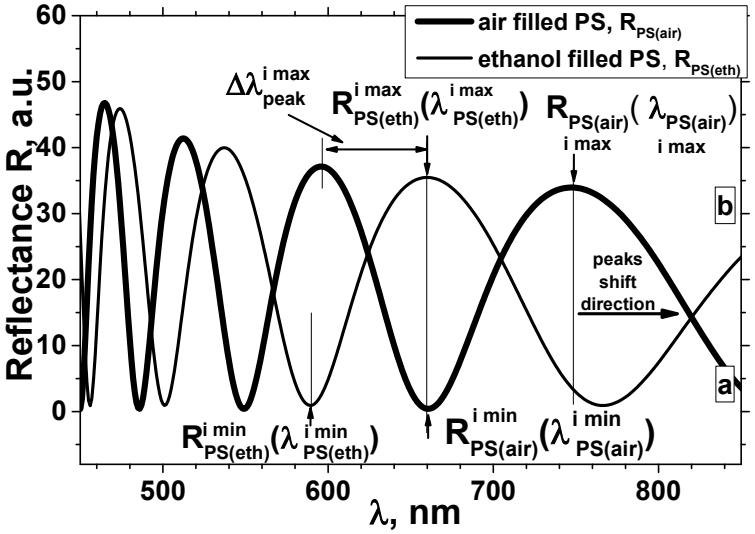

Fig. 5. Simulated spectral dependence of reflectance $R_{PS(air)}$ of air (a) and reflectance $R_{PS(eth)}$ of ethanol (b) filled PS layer (PS layer thickness L_{PS}=500 nm, porosity P=70%) .

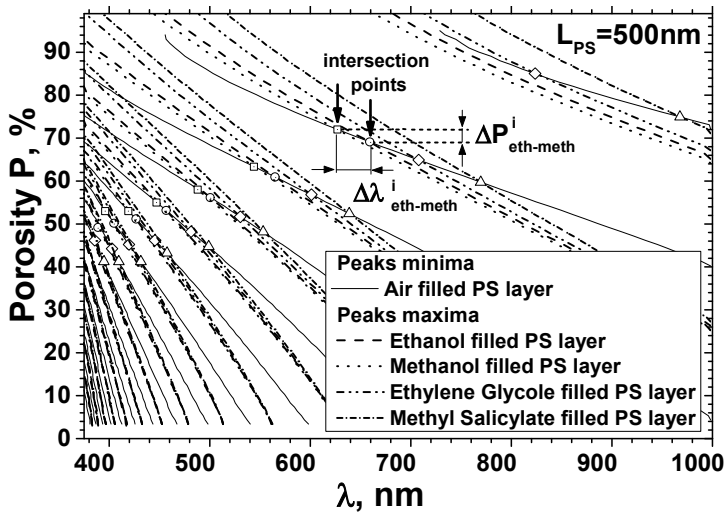

Fig. 6. Dependence of interference peaks of reflectance minima position of nonfilled PS layer and peaks of reflectance maxima position for filled PS layer by ethanol, methanol, ethylene glycol, methyl salicylate versus porosity and wavelength λ (PS layer thickness L_{PS}=500 nm)

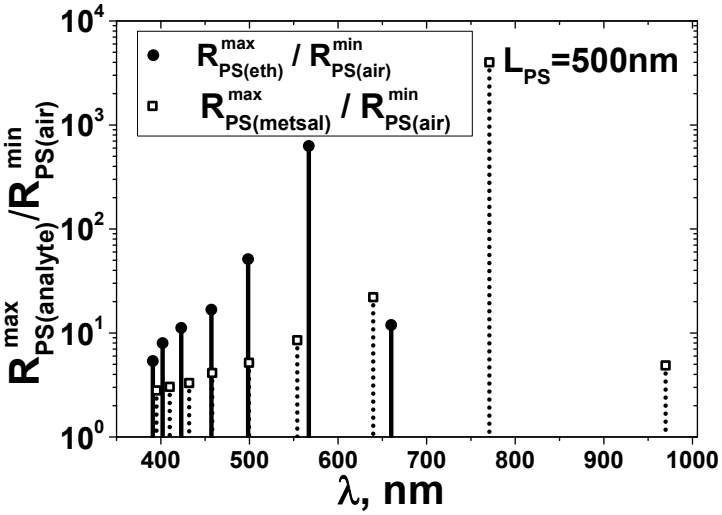

Fig.7. Ratio of reflectance for filled PS layer by ethanol ($R^{i\max}_{PS(eth)}$) and methyl salicylate ($R^{i\max}_{PS(metsal)}$) to reflectance for nonfilled PS layer ($R^{i\min}_{PS(air)}$) as function of λ. Here $\lambda^{i\max}_{PS(eth)} = \lambda^{i\min}_{PS(air)}$ and $\lambda^{i\max}_{PS(metsal)} = \lambda^{i\min}_{PS(air)}$, respectively (b).

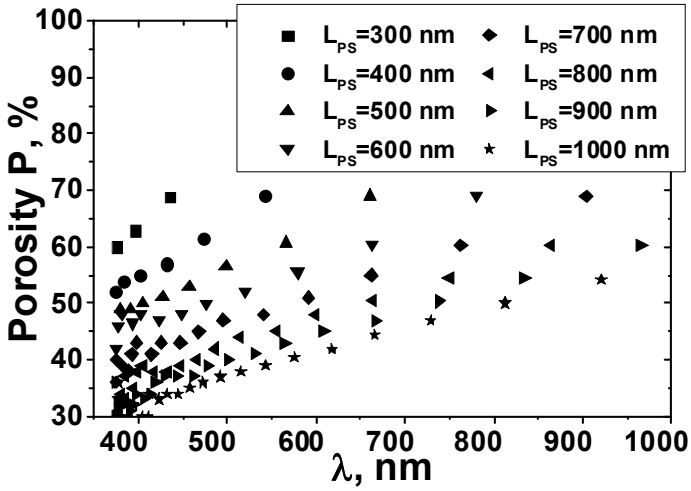

Fig. 8. Position of points where interference peaks of maximum $\lambda^{i\max}_{PS(eth)}$ for ethanol filled PS layers equal to interference peaksof minima for nonfilled PS layers $\lambda^{i\min}_{PS(air)}$ at different PS layer thickness L_{PS}.

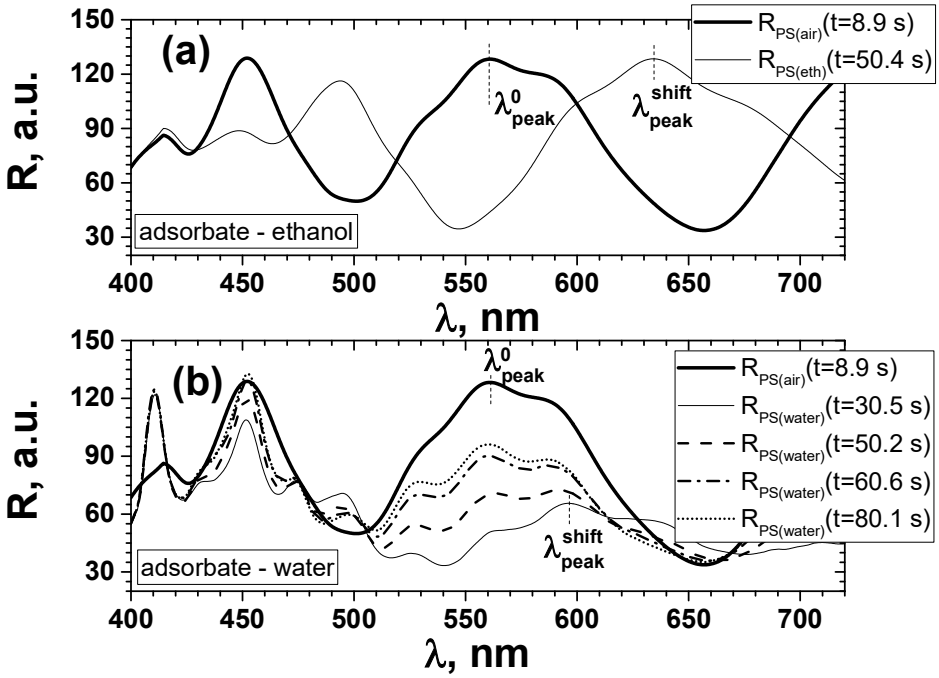

Fig. 9. The dependence of the reflection coefficient of the structure with nonfilled and filled by ethanol pores on the wavelength at different times (a). The dependence of the reflection coefficient of the structure with nonfilled and filled by water pores on the wavelength at different times (b).

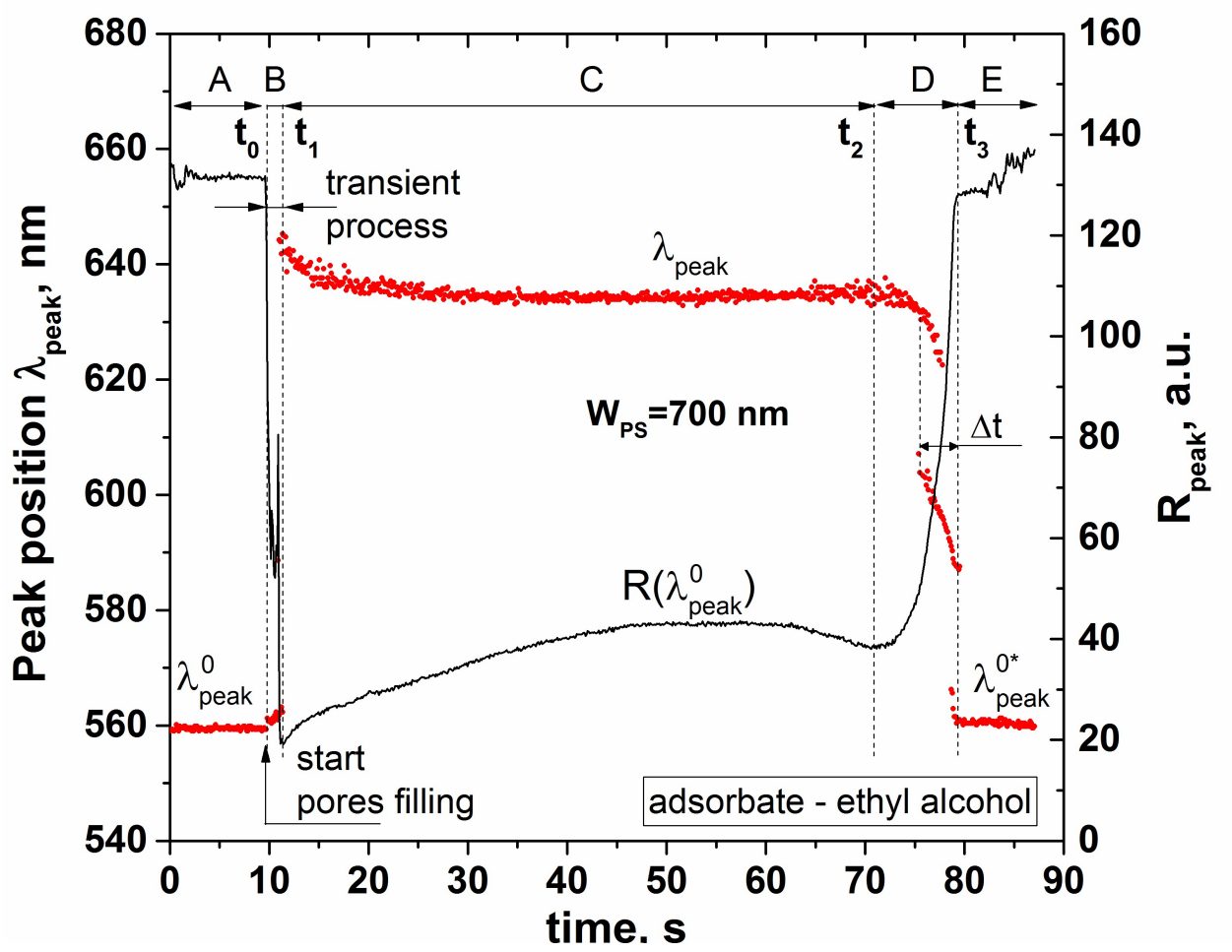

Fig. 10. Dependence of the maximum position of the interference peak λ_{peak} and the reflection coefficient ($R(\lambda^0_{peak} = const)$ on the time after covering of the sample surface by ethyl alcohol.

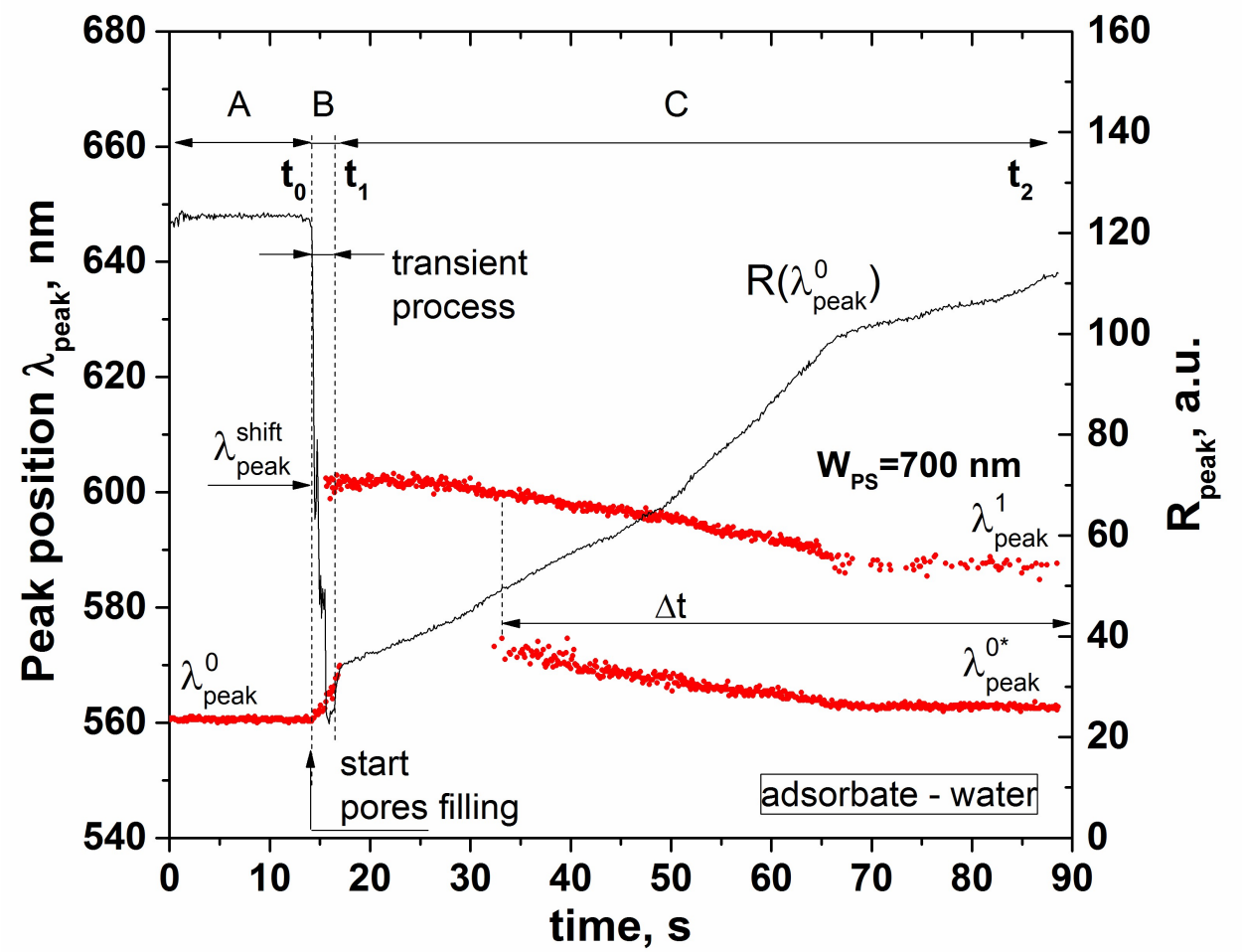

Fig. 11. Dependence of the maximum position of the interference peak λ_{peak} and the reflection coefficient $R(\lambda^0_{peak} = const)$ on the time after covering of the sample surface by distilled water. Note: during the desorption of water from pores the part of the water molecules is remained in the pores of the PS. It leds to the splitting of the interference peak and the decreasing of the reflection coefficient $R_{peak.}$

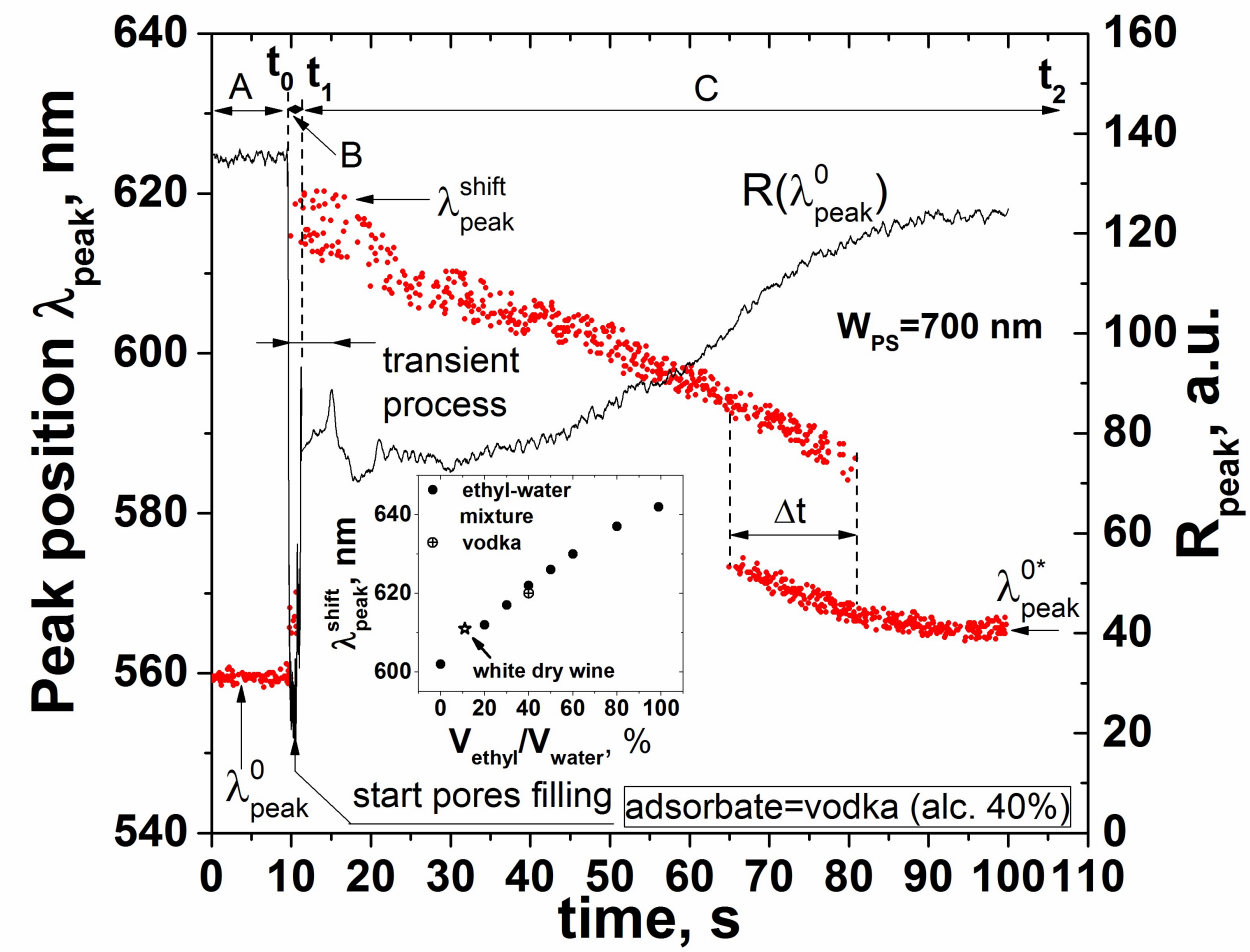

Fig. 12. Dependence of the maximum position of the interference peak λ_{peak} and the reflection coefficient ($R(\lambda^0_{peak} = const)$ on the time after covering of the sample surface by vodka (Nemiroff®, alcohol 40%). Inset: dependence of maximum position of the interference peak λ^{shift}_{peak} on ethyl to water volume ratio after covering of the sample surface by ethyl-vodka ratio. Peak position λ^{shift}_{peak} for vodka (alcohol 40%) and white dry wine (alcohol 9..13%, sugar 2..3 g/dm^3) is shown for comparison.

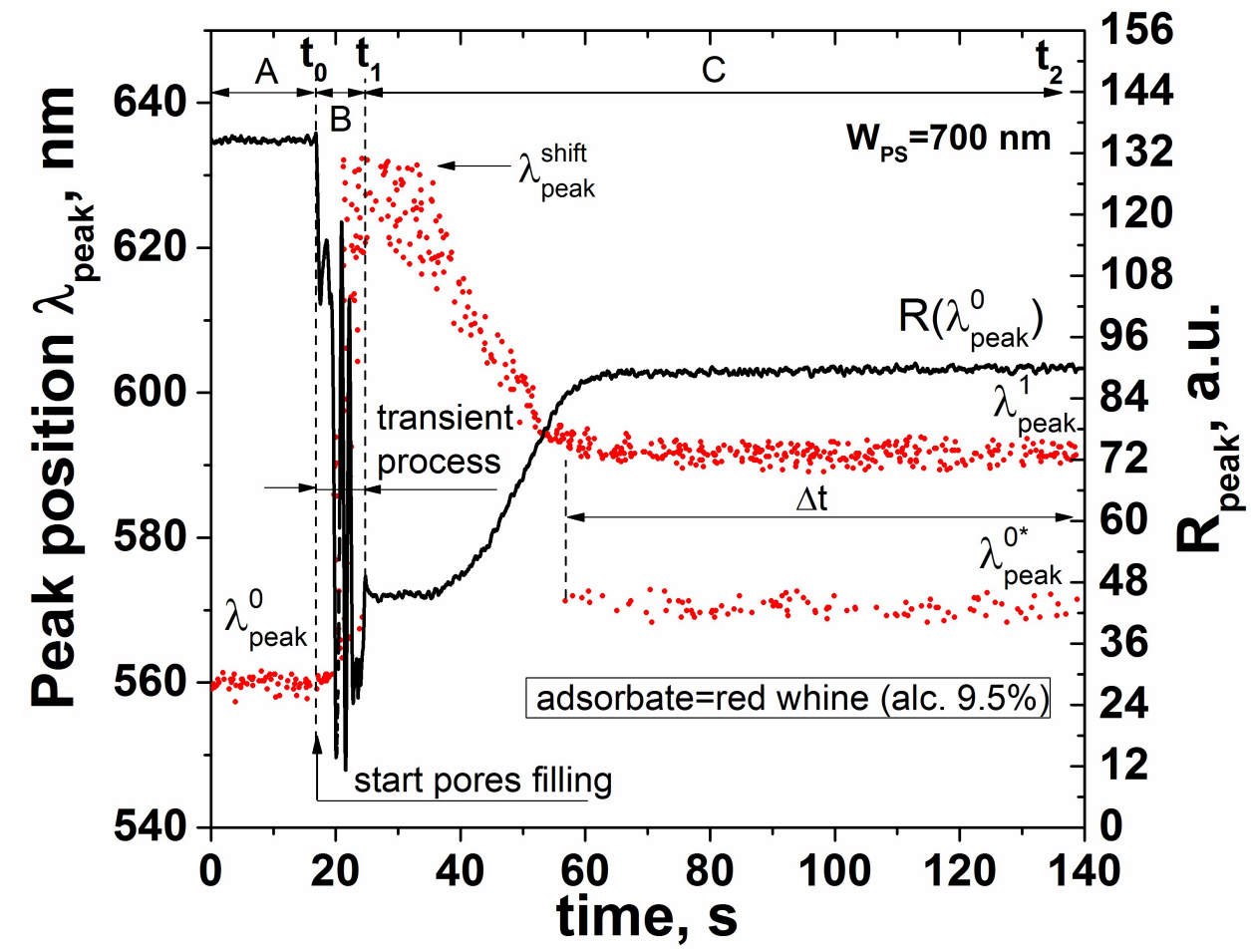

Fig. 13. Dependence of the maximum position of the interference peak λ_{peak} and the reflection coefficient ($R(\lambda^0_{peak} = const)$ on the time after covering of the sample surface by red wine (Cabernet, alcohol - 9.5%, sugar - 18 g/dm^3).

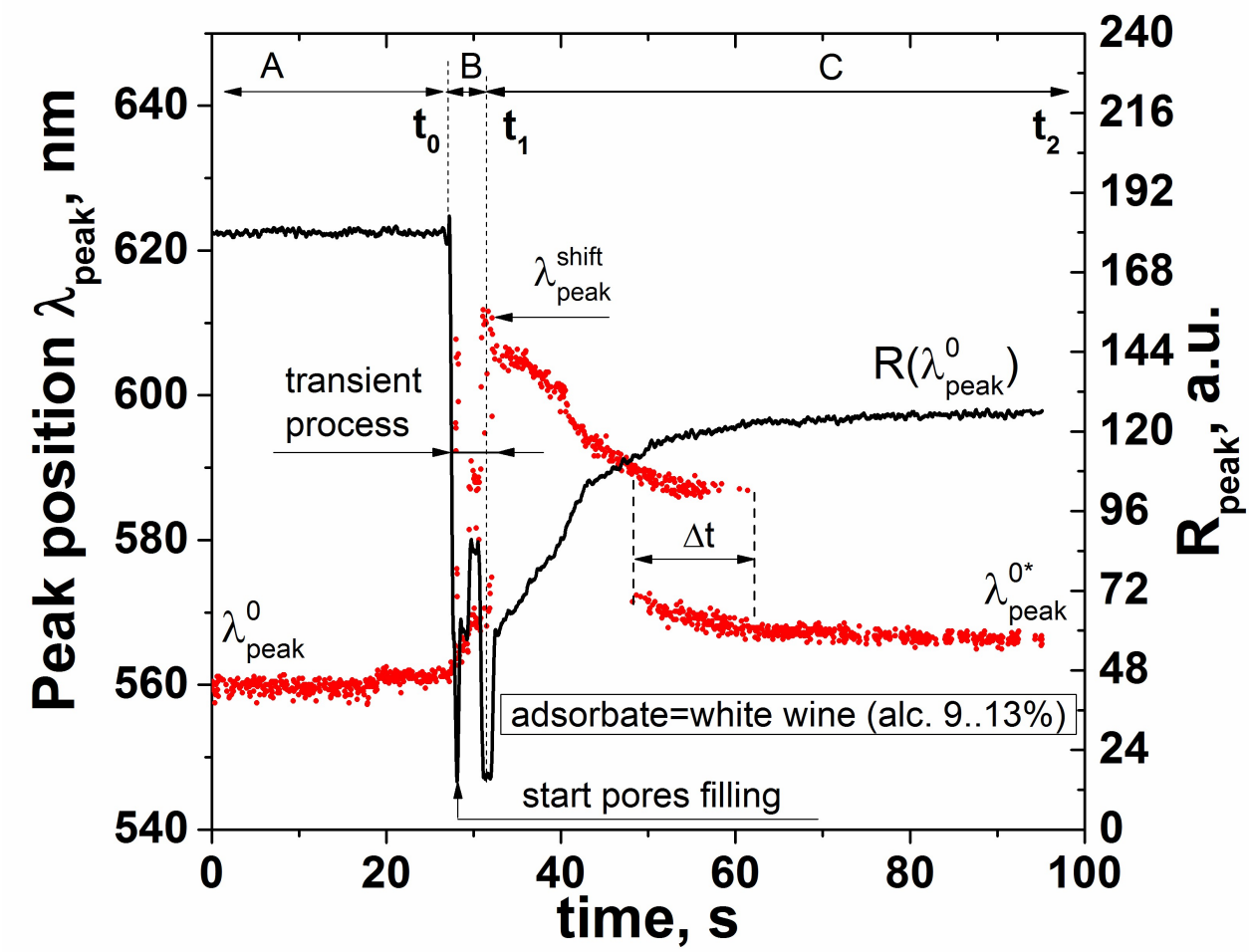

Fig. 14. Dependence of the maximum position of the interference peak λ_{peak} and the reflection coefficient ($R(\lambda^0_{peak} = const)$ on the time after covering of the sample surface by white wine (Cabernet, alcohol - 9..13%, sugar - 2..3 g/dm^3).